



Interfacial reactions and mechanical properties of Sn–3.0Ag–0.5Cu solder with pure Pd or Pd(P) layers containing thin-Au/Pd/Ni(P) surface-finished PCBs during aging

Jungsoo Kim^{1,2} · Jong-Hoon Back¹ · Seung-Boo Jung² · Jeong-Won Yoon¹

Received: 19 November 2019 / Accepted: 20 January 2020 / Published online: 29 January 2020
© Springer Science+Business Media, LLC, part of Springer Nature 2020

Abstract

The microelectronics packaging industry, although rapidly growing, faces several challenges including 3-D integration, issues with multifunctional capability, and fluctuating input/output (I/O) density, among others. Better-performing microelectronics assemblies for mitigating these challenges require alloys with superior solderability and minimal metallization layer thickness. To this end, in this study, we investigated two kinds of electroless-nickel electroless-palladium immersion gold (ENEPIG) with 0.3 μm Ni, 0.1 μm pure Pd or Pd-phosphorous (Pd(P)), and 0.1 μm Au layers plated on a printed circuit board (PCB) substrate. To analyze the effects of the pure Pd and Pd(P) layers in the thin ENEPIG, we evaluated the interfacial reactions and mechanical properties of the SAC305 solder with a pure Pd or Pd(P) layer in the thin ENEPIG joints after aging at 150 °C. Needle-type and chunky-type $(\text{Cu,Ni})_6\text{Sn}_5$ IMCs were formed at the interfaces of the pure Pd and Pd(P) joints, respectively. The $(\text{Cu,Ni})_6\text{Sn}_5$ IMC of the pure Pd joint was thinner than that of the Pd(P) joint after reflowing and aging for 100 h. However, the total IMC of the Pd(P) joint was thinner than that of the pure Pd joint from 250 to 1000 h. In a low-speed shear test, the shear strength of the Pd(P) joint was higher than that of the pure Pd joint for the entire aging time. Most fractures occurred at the Sn-rich surface with a ductile mode, regardless of the different substrates and aging times. After high-speed shear testing, the shear strength of the pure Pd joint was higher than that of the Pd(P) joint until aging for 100 h. After aging for 250 h, the shear strength of the Pd(P) joint was higher than that of the pure Pd joint. The results for brittle fracture rate were similar to those for high-speed shear strength. Hence, Pd(P) joints are expected to demonstrate higher reliabilities than pure Pd joints after long aging treatment.

1 Introduction

The microelectronics packaging industry has continuous demands for advanced device performance such as miniaturization, 3-D integration, multifunctional capability, and high input/output (I/O) density [1, 2]. These performances depend on factors of highly reliable interconnections and fine-pitch process during microelectronic assembly [3–5].

Therefore, superior solderability and minimal metallization layer thickness have critical issues for joining technology. As such, thin surface finishes with high joint reliability contribute to fine-pitch and low-cost manufacturing.

In the early 2000s, eutectic Sn–Pb solder was banned as a part of restrictions on the use of certain hazardous substances (RoHS) and waste electrical and electronic equipment (WEEE) owing to the toxicity of Pb, which is harmful for humans and causes environment pollution [6, 7]. Therefore, many kinds of Pb-free solder alloys have been developed to replace the Sn–Pb solder used in microelectronics. Most Pb-free solder alloys are Sn-base ones such as Sn–Ag, Sn–Ag–Cu, Sn–Cu, Sn–Bi, and Sn–Ni solder families [8–21]. Among these, Sn–Ag–Cu is the most favorable solder alloy due to its excellent characteristics, including good wettability, high creep resistance, low coarsening rate, and long-term reliability [22–26].

In addition, various surface finishes have been used to increase joint reliability, including immersion Ag,

✉ Seung-Boo Jung
sbjung@skku.edu

✉ Jeong-Won Yoon
jwoon@kitech.re.kr

¹ Welding and Joining R&D Group, Korea Institute of Industrial Technology (KITECH), 156 Gaetbeol-ro, Yeonsu-gu, Incheon 21999, Korea

² School of Advanced Materials Science & Engineering, Sungkyunkwan University, 2066 Seobu-ro, Jangan-gu, Suwon 16419, Gyeonggi-do, Korea

immersion Sn, organic solderability preservative (OSP), and electroless-nickel immersion gold (ENIG). An OSP surface finish is used mainly to prevent Cu oxidation and has a competitive price [27–29]. An ENIG surface finish has excellent wettability and retards intermetallic compound (IMC) growth [30, 31]. In the ENIG system, the Au layer improves the wettability and the Ni layer plays the role of a diffusion barrier for Cu atoms. However, galvanic hyper-corrosion of the Ni layer leads to the “black pad” phenomenon, which can degrade the reliability of the solder joints [31–33]. To enhance the reliability of the ENIG surface finish, the electroless-nickel electroless-palladium immersion gold (ENEPIG) surface finish has been developed. A Pd layer is placed between the Au and Ni layers; this layer acts as a diffusion barrier and wetting layer [34–38]. In the Pd layer plating process, the phosphorus (P) is mostly used as a reduction agent [39]. There are two methods for plating the Pd layer on the Ni(P) layer. The pure Pd (crystalline) and Pd(P) (amorphous) layers are formed using formic acid and hypophosphorous acid, respectively. These methods are the most commonly used plating methods for the Pd layer in the ENEPIG surface finishing process. To improve the productivity of the ENEPIG surface finish, thin ENEPIG surface-finished printed circuit boards (PCBs) have been developed [40, 41]. However, research comparing the use of pure Pd or Pd(P) in the ENEPIG surface finish is lacking.

In this study, we investigated the effects of phosphorus (P) in the Pd layer of thin ENEPIG PCBs with a Sn–3.0Ag–0.5Cu (SAC305) solder joint. For this purpose, the interfacial reactions and mechanical properties of the SAC305 solder joints with a pure Pd or Pd(P) layer in the thin ENEPIG PCB joints (pure Pd or Pd(P) joints) were investigated after reflowing and aging treatments.

2 Experimental

In this study, two kinds of Pd layer structures contained within the thin ENEPIG surface finish were investigated. The thin ENEPIG surface finish was composed of a 0.3 μm Ni(P), 0.1 μm pure Pd or Pd(P), and a 0.1 μm Au layer on the Cu PCB substrate. The sequence of the ENEPIG surface finishing process is as follows: cleaning—soft etching—acid dipping—pre-dipping—catalysis at the Cu and Ni interface—post dipping—electroless Ni(P)—electroless Pd or Pd(P)—immersion Au. Each step during the ENEPIG surface finishing process has different processing temperatures and dipping times to achieve optimized plating properties. In the Pd layer plating process, two kinds of Pd layer, pure Pd and Pd(P), were formed using formic acid and hypophosphoric acid, respectively. The pure Pd and Pd(P) layers were plated at 65 $^{\circ}\text{C}$ and 50 $^{\circ}\text{C}$, respectively, for 10 min. The PCB substrate was a surface-mounted

device (SMD)-type flame-retardant-4 (FR-4). The SAC305 solder paste (M705-GRN360-K2-V, Senju Metal Industry Co. Ltd., Japan) was printed on the ENEPIG-plated Cu pad using a screen-printing method. After printing, SAC305 solder balls (Duksan Hi-Metal Co. Ltd., Korea) were placed on the printed SAC305 solder paste. The diameter of each SAC305 solder ball was 450 μm and that of the Cu pad opening on the PCB was 350 μm . The reflow process was then performed at a peak temperature of 260 $^{\circ}\text{C}$ for 5 min using a reflow machine (Heller Co. Ltd., USA). The reflow profile is shown in Fig. 1. After the reflow process, samples were cooled at room temperature and the flux was removed using a deflux solution and alcohol. The pure Pd and Pd(P) joints were aged at 150 $^{\circ}\text{C}$ for 100, 250, 500, and 1000 h. The microstructures and fracture surfaces of the pure Pd and Pd(P) joints were examined using an electron probe micro analyzer (EPMA, SX-100, CAMECA, USA) and a scanning electron microscope (SEM, INSPECT F, FEI, USA). The chemical compositions of these solder joints were determined by energy-dispersive spectroscopy (EDS). The mechanical strengths of the pure Pd and Pd(P) joints were evaluated using global low-speed and high-speed ball shear testers (DAGE-4000 and DAGE-4000HS, Nordson DAGE, UK). A schematic diagram of the ball shear tests is shown in Fig. 2. The conditions of shear testing were 50 μm of shear height and 200 $\mu\text{m}/\text{s}$ and 1 m/s of shear speed in compliance with the Joint Electron Device Engineering Council (JEDEC) standard 22-B117A.

3 Results and discussion

Figure 3 shows the cross-sectional SEM micrographs of the pure Pd and Pd(P) joints after reflowing. A needle-type $(\text{Cu},\text{Ni})_6\text{Sn}_5$ IMC and P-rich Ni layers were formed at the interface between the SAC305 solder and the pure Pd joint, as shown in Fig. 3a. The composition of this IMC layer was determined to be 17.45 at.% Ni, 39.5 at.% Cu, and 43.05 at.% Sn. In general, the Au and Pd layers which were plated on the

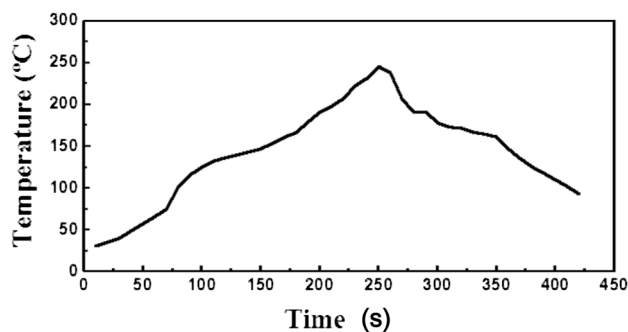


Fig. 1 Reflow temperature profile

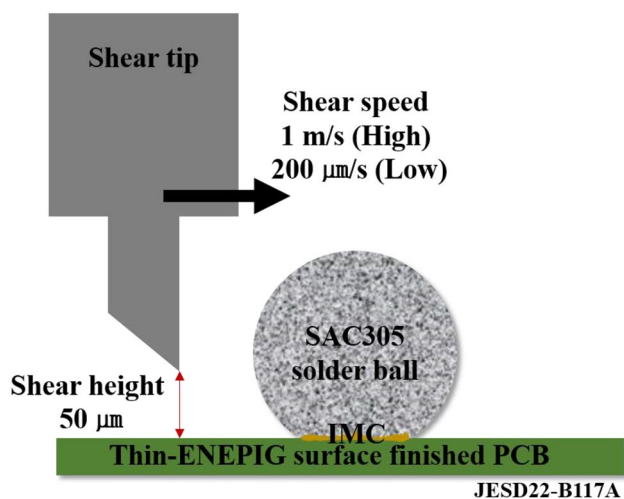


Fig. 2 Schematic diagram of ball shear test

Ni(P) layer in the ENEPIG surface finish were rapidly dissolved into the SAC solder during the reflow process. Then, Sn and Cu in the SAC solder and Ni in the surface-finished PCB substrate reacted and formed $(\text{Cu,Ni})_6\text{Sn}_5$ which was the dominant IMC at the interface between Cu-containing Sn-rich solder and the thin ENEPIG joint after reflowing and aging. In contrast, chunky-type $(\text{Cu,Ni})_6\text{Sn}_5$ IMCs formed at the interface between the SAC305 solder and Pd(P) joints after reflow (Fig. 3b). Unlike the $(\text{Cu,Ni})_6\text{Sn}_5$ IMC of the pure Pd joint that only formed at the top of the interface, the $(\text{Cu,Ni})_6\text{Sn}_5$ IMC of the Pd(P) joints formed at the top and bottom of the interface between the SAC 305 solder and Cu substrate. During the reflow reaction, the Ni(P) layer was almost consumed, and the P-rich Ni layer that was formed

was partially destroyed by molten solder. As a result, the molten solder reacted with the Cu substrate and formed the IMC under the P-rich Ni layer.

Figure 4 shows the cross-sectional SEM micrographs of the pure Pd joints after aging at 150 °C for up to 1000 h. The P-rich Ni layer formed at the interface between the $(\text{Cu,Ni})_6\text{Sn}_5$ IMC and Cu substrate until aged for 100 h. After aging for 250 h, only the $(\text{Cu,Ni})_6\text{Sn}_5$ IMC remained at the interface, as shown in Fig. 4c. It is interesting to note that the interfacial IMC thickness rapidly increased between 100 and 250 h due to the fast diffusion of Cu to form the $(\text{Cu,Ni})_6\text{Sn}_5$ IMC layer. Therefore, the $(\text{Cu,Ni})_6\text{Sn}_5$ IMC layer rapidly grew toward the direction of the solder after 100 h of aging. During prolonged aging for 1000 h, the $(\text{Cu,Ni})_6\text{Sn}_5$ IMC layer continued to thicken. The Cu in the substrate was continuously supplied toward the interface and then the $(\text{Cu,Ni})_6\text{Sn}_5$ IMC grew toward the direction of the solder. A relatively flat interface between the $(\text{Cu,Ni})_6\text{Sn}_5$ IMC layer and the Cu substrate was observed in the pure Pd joint, as shown in Fig. 4.

Markedly different interfacial microstructures are observed in the Pd(P) joints. Figure 5 shows the cross-sectional SEM micrographs of the Pd(P) joints after aging at 150 °C for up to 1000 h. The top and bottom of the $(\text{Cu,Ni})_6\text{Sn}_5$ IMCs gradually increased with aging time in both directions. Compared with the pure Pd joint (Fig. 4), the top and bottom of the $(\text{Cu,Ni})_6\text{Sn}_5$ IMCs became simultaneously more coarse at the interface of the Pd(P) joint in the direction of both the solder and substrate. In addition, the IMC interface was rough and uneven.

The total IMC thicknesses of the pure Pd and Pd(P) joints as a function of aging time are shown in Fig. 6. After reflow, the IMC thicknesses of the pure Pd and Pd(P) joints

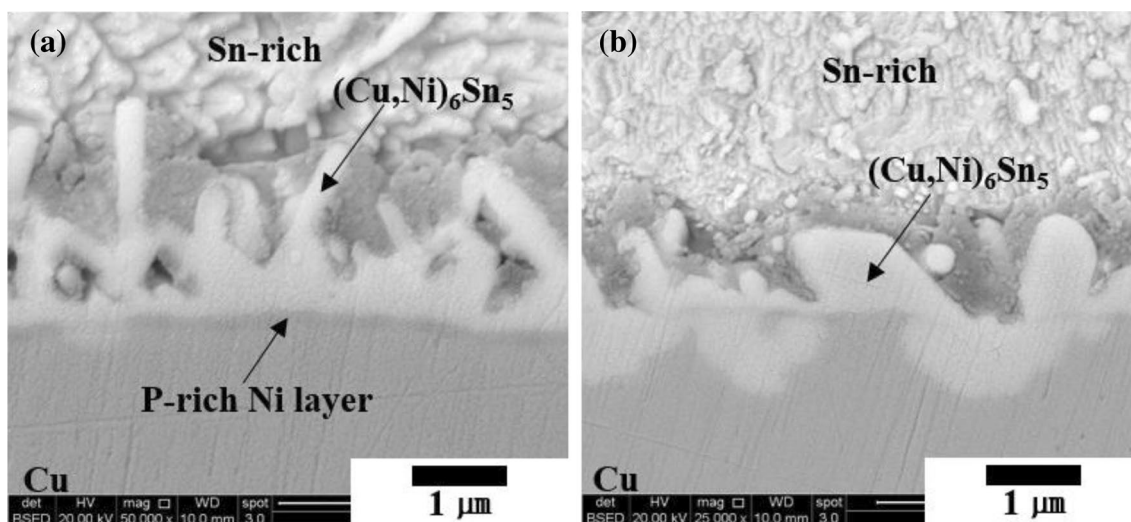


Fig. 3 Cross-sectional SEM micrographs of Sn-3.0Ag-0.5Cu solder with **a** pure Pd and **b** Pd(P) containing thin ENEPIG surface-finished PCB joints after reflow

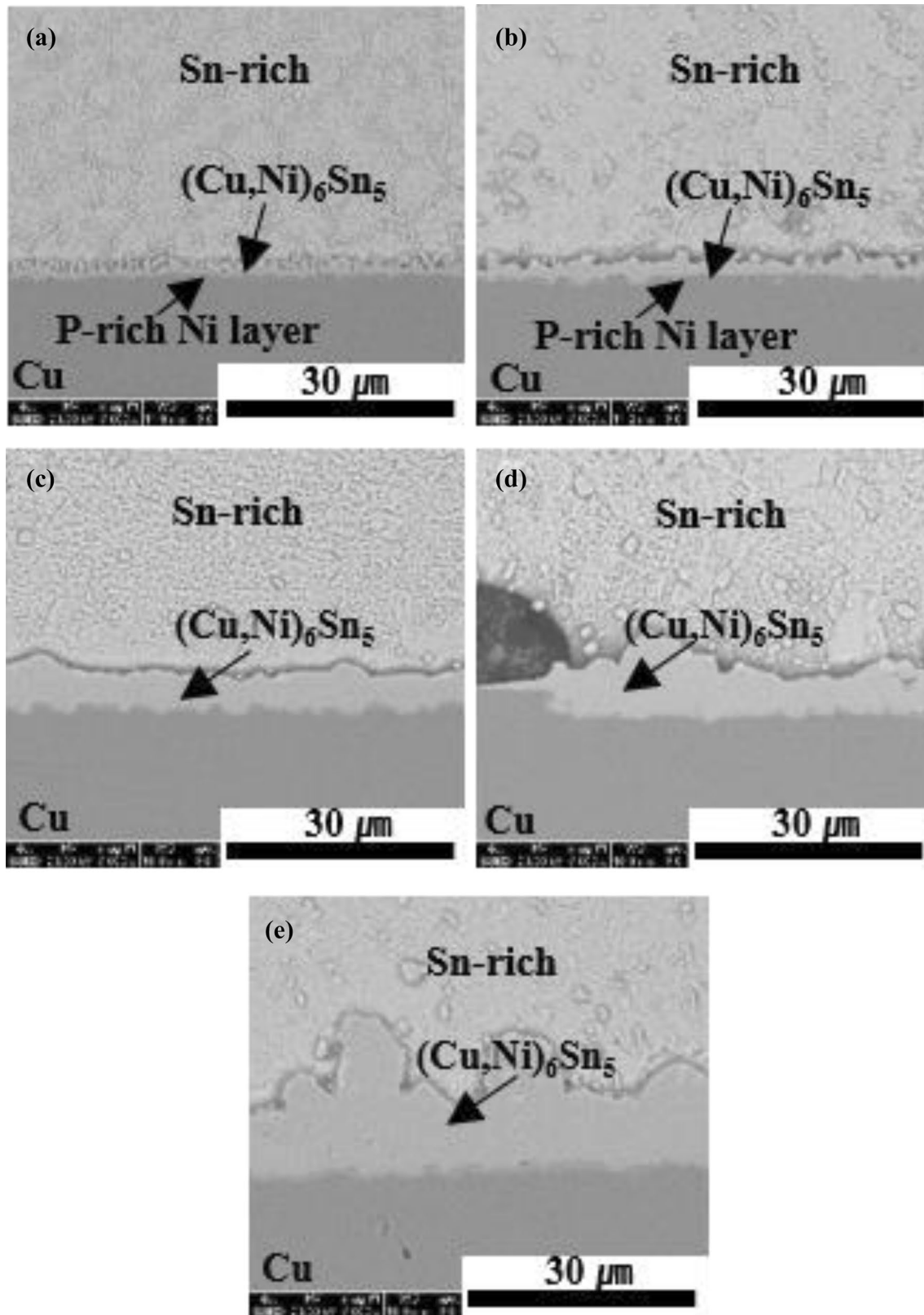


Fig. 4 Cross-sectional SEM micrographs of Sn–3.0Ag–0.5Cu solder with pure Pd containing thin ENEPIG surface-finished PCB joints after aging at 150 °C. After **a** reflow, **b** 100 h, **c** 250 h, **d** 500 h, and **e** 1000 h

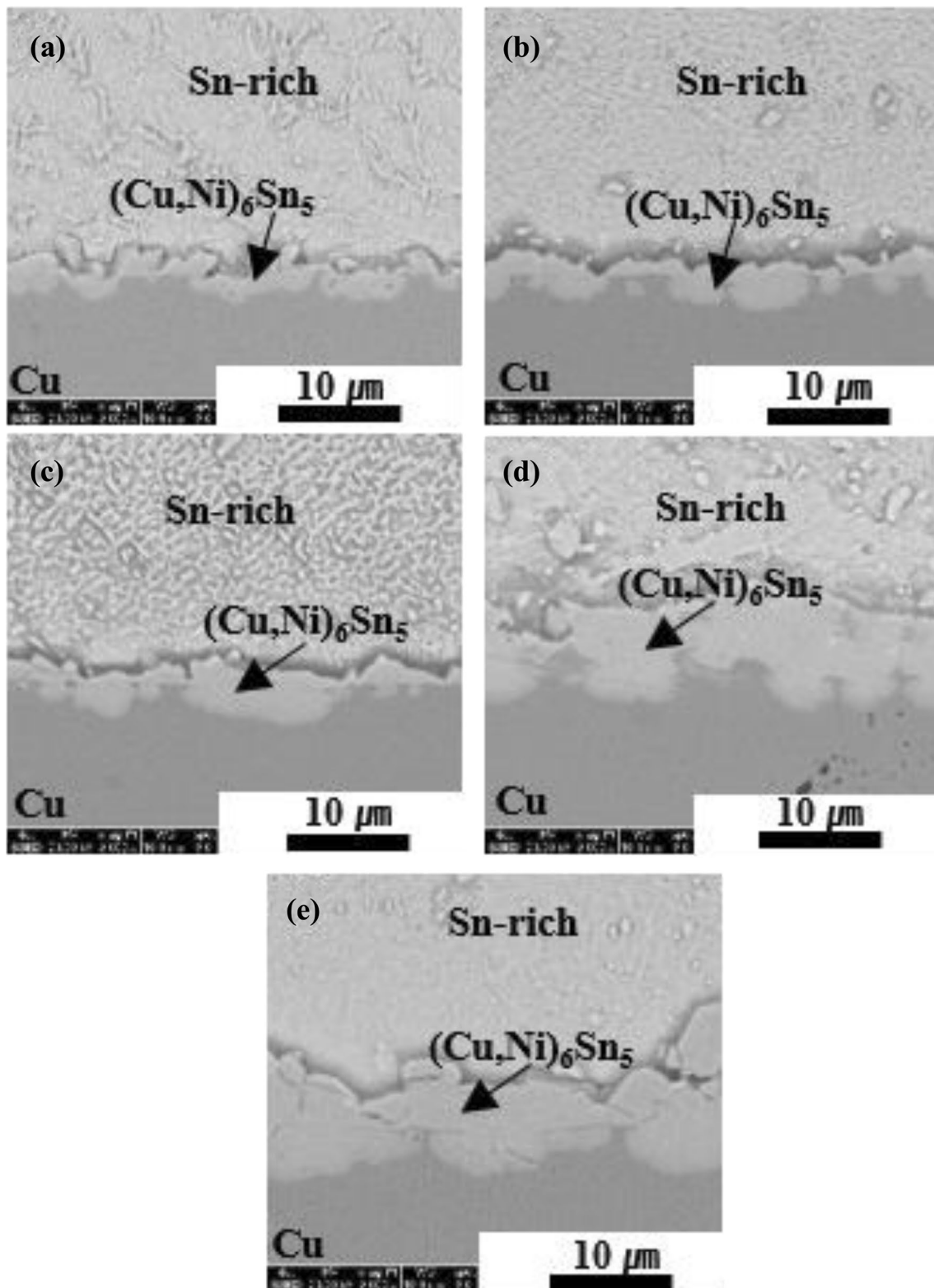


Fig. 5 Cross-sectional SEM micrographs of Sn–3.0Ag–0.5Cu solder with Pd(P) containing thin ENEPIG surface-finished PCB joints after aging at 150 °C. After **a** reflow, **b** 100 h, **c** 250 h, **d** 500 h, and **e** 1000 h

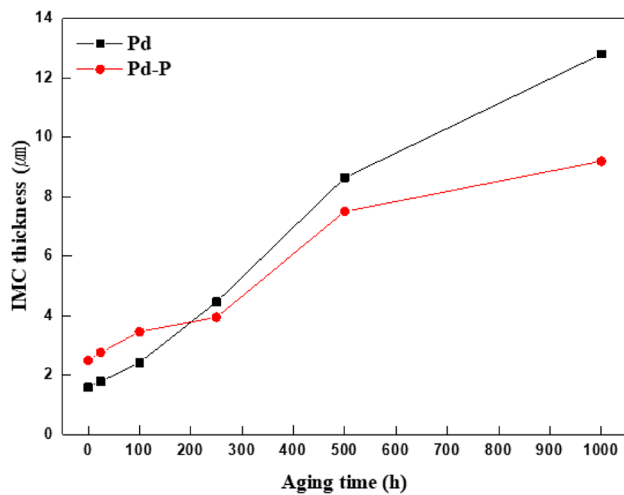


Fig. 6 Total IMC thickness as a function of aging time at 150 °C for Sn–3.0Ag–0.5Cu solder with pure Pd and Pd(P) containing thin ENEPIG surface-finished PCB joints

were 1.59 and 2.49 μm , respectively. The $(\text{Cu,Ni})_6\text{Sn}_5$ IMC thicknesses of both pure Pd and Pd(P) joints increased with increasing aging time. The IMC of the Pd(P) joint was thicker than that of the pure Pd joint up to an aging time of 100 h. However, the IMC growth rate of the Pd(P) joint slightly decreased between 100 and 250 h of aging, while that of the pure Pd joint increased rapidly. As a result, the IMC of the pure Pd joint was thicker than that of the Pd(P) joint after aging between 250 to 1000 h. After aging for 1000 h, the IMC of the pure Pd joint was approximately 1.4 times thicker than that of the Pd(P) joint.

Figures 7a and b show the cross-sectional EPMA mapping results of the pure Pd joints after aging at 150 °C for 100 and 250 h, respectively. The P, which was contained in the Ni(P) layer, was detected on the Cu substrate. In addition, a relative abundance of Ni was detected between the $(\text{Cu,Ni})_6\text{Sn}_5$ IMC and the Cu substrate. Au and Pd were not observed at the joint interface because these elements were already completely dissolved into the solder during the reflow process. The $(\text{Cu,Ni})_6\text{Sn}_5$ IMC layer mainly grew toward the SAC305 solder during the 100 h of aging. After 250 h, the $(\text{Cu,Ni})_6\text{Sn}_5$ IMC had grown rapidly toward the direction of the SAC solder and most of the Ni was still located at the bottom of the interface. From the Ni elemental mapping image, we confirmed the position of the original Ni/Cu interface and the direction of growth of the IMC layer toward the SAC solder. The P-rich Ni was simultaneously destroyed by diffusion of Sn and Cu into the Cu substrate and Sn-rich solder of pure Pd and Pd(P) joint. As a result, the growth rates of the IMC layer for both pure Pd and Pd(P) joints rapidly increased after aging for 250 h.

Compared with the pure Pd joint, the Pd(P) joint showed a different microstructure (Fig. 8). Some Ni was detected in

the middle of the interface, and Sn diffused into the Cu substrate. The location of Ni reflected the original Ni/Cu interface. As a result, the $(\text{Cu,Ni})_6\text{Sn}_5$ IMC layer grew toward both the SAC305 solder and the Cu pad. The P-rich Ni layer was partially destroyed by the induced rapid diffusion of Sn into the Cu substrate of the Pd(P) joint. As a result, a part of the P-rich Ni layer was consumed to form $(\text{Cu,Ni})_6\text{Sn}_5$ IMC at the interface of the pure Pd joint after aging for 100 h. However, at the interface of the pure Pd joint, the P-rich Ni layer, after aging for 100 h, was thicker than that of the Pd(P) joint which was almost destroyed, owing to the formation of the top and bottom layers of $(\text{Cu,Ni})_6\text{Sn}_5$ IMC. In addition, the dimension and thickness of the P-rich Ni layer at the interface of the pure Pd joint after aging for 100 h were greater than after 250 h of aging.

Figure 9 shows the schematic diagrams of sequential interfacial reactions at the pure Pd and Pd(P) joints with aging time. As shown in Fig. 9a, the Cu in the Cu substrate diffused toward the solder matrix only after aging. The diffusion of Cu toward the SAC solder was prominent, regardless of the P-rich Ni layer on the Cu substrate. As a result, the $(\text{Cu,Ni})_6\text{Sn}_5$ IMC layer only grew in the direction of the solder. For these reasons, the Cu was the main diffusion element for the growth of the interfacial $(\text{Cu,Ni})_6\text{Sn}_5$ IMC layer of the pure Pd joint. In contrast, the $(\text{Cu,Ni})_6\text{Sn}_5$ IMC layer of the Pd(P) joint (Fig. 9c) grew toward both the solder and the Cu substrate, and its thickness was greater than that of the pure Pd joint at reflowing and initial aging. The cause of the thicker IMC layer of the Pd(P) joint compared to the pure Pd joint was the formation of chunky-type $(\text{Cu,Ni})_6\text{Sn}_5$ IMCs and rapid Sn diffusion due to the partial destruction of the P-rich Ni layer in the Pd(P) joint. The Sn diffused into the valleys of the chunky-type $(\text{Cu,Ni})_6\text{Sn}_5$ IMCs to form IMCs at the bottom of the interface that grew toward the Cu substrate. As well as Sn, Cu diffused under aging. Therefore, Sn was the main diffusion element in the Pd(P) joint. On the other hand, in the pure Pd joint after long-term aging (Fig. 9b), Cu was the main diffusion element and the interfacial IMC layer grew continuously with increasing aging time. In addition, the P-rich Ni layer became exhausted at the interface after a long duration of aging because the bottom of the $(\text{Cu,Ni})_6\text{Sn}_5$ IMC grew at the location of the P-rich Ni layer. P-rich Ni layers act as diffusion barriers to Cu atoms moving toward the Sn-rich solder [42]. However, consumption of the P-rich Ni layer at the joint facilitated Cu diffusion from the Cu substrate. As a result, relatively thick interfacial IMCs formed at the pure Pd joint after aging for 250 h. We indicated the growth directions of the interfacial IMC layer and original Ni/Cu interfaces using black arrows and pink-colored lines, respectively, in Fig. 9.

Figure 10 shows the high-speed (a) and low-speed (b) shear strengths of the pure Pd and Pd(P) joints as a function of aging time. As shown in Fig. 10a, the high-speed shear

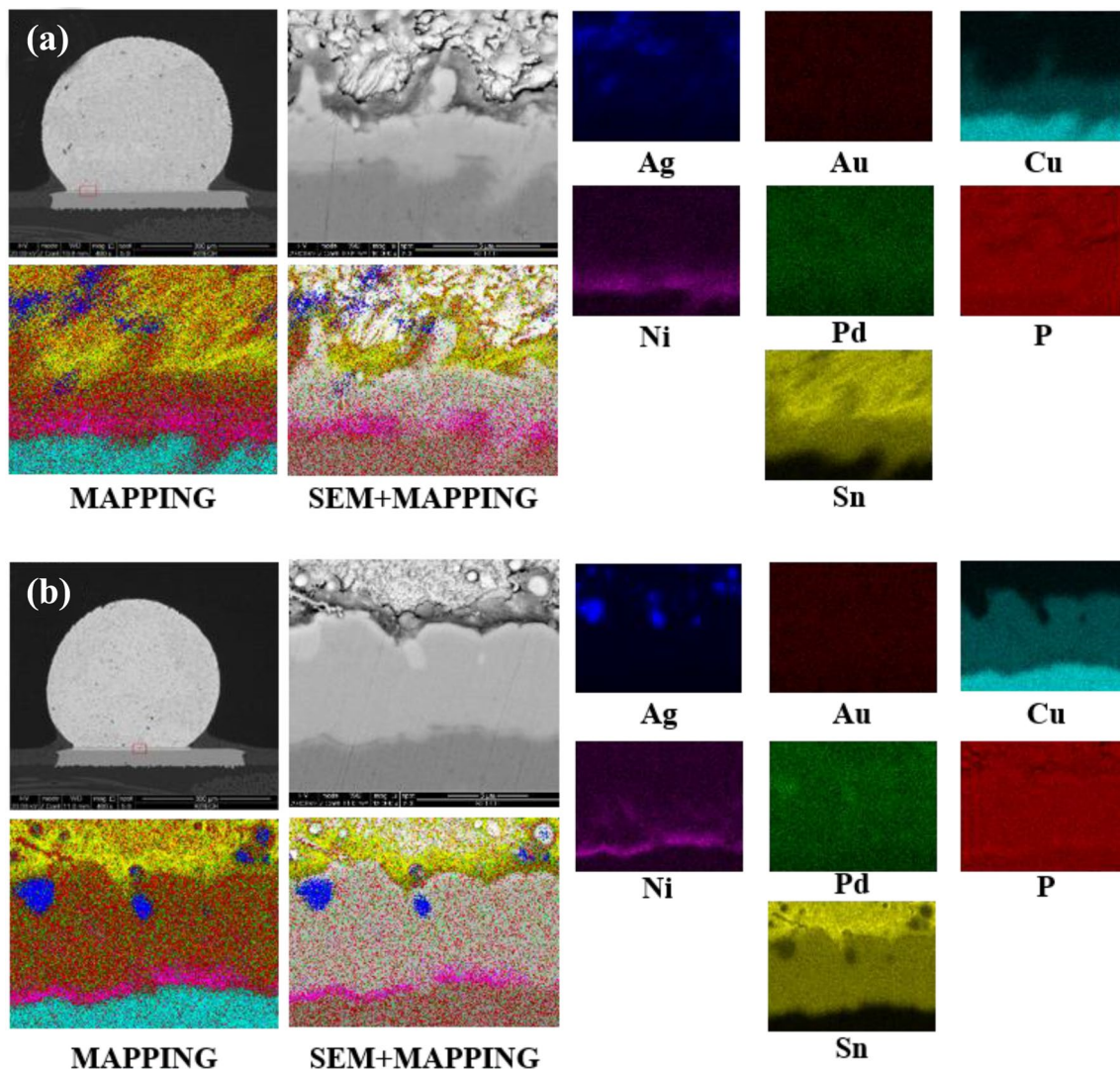


Fig. 7 SEM elemental mapping of Sn-3.0Ag-0.5Cu solder with pure Pd containing thin ENEPIG surface-finished PCB joints after aging at 150 °C. **a** 100 h and **b** 250 h

strength of the pure Pd joint was slightly higher than that of the Pd(P) joint up to an aging time of 100 h. The high-speed shear strength of both the pure Pd and Pd(P) joints rapidly decreased after 100 h of aging. In addition, the high-speed shear strength of the Pd(P) joint was slightly higher than that of the pure Pd joint after aging for 250 h. There was a crossing point between 100 and 250 h. These results are consistent with the IMC thickness result (Fig. 6), which explains why the shear strengths measured by high-speed shear tests as a type of impact testing, and were closely related to the interfacial IMC thickness. Similar results have been reported in the literature [41–43]. After aging for 500 h, the shear strengths of both solder joints were not significantly changed.

Low-speed shear strength variations of the pure Pd and Pd(P) joints during aging are shown in Fig. 10b. The

low-speed shear strength of the SAC solder joints with pure Pd and Pd(P) joints decreased with increasing aging time. In particular, the shear strength for both joints significantly decreased after aging for 24 h. However, the shear strength of the Pd(P) joint was slightly higher than that of the pure Pd joint, regardless of aging time.

Figure 11 shows the top view SEM micrographs of the pure Pd and Pd(P) joints after high-speed shear testing. The fracture surface of the pure Pd joint after reflow (Fig. 11a) was mostly a Sn-rich matrix with a ductile mode. Part of the fracture surface was observed at the P-rich Ni layer, but most of the fracture surface was the Sn-rich solder up to 100 h (Fig. 11b). However, both the $(\text{Cu,Ni})_6\text{Sn}_5$ IMC and solder surface featured at the fracture surface after 250 h. As shown in Fig. 11(d-e), the $(\text{Cu,Ni})_6\text{Sn}_5$ IMC occupied more than 60% of the total fracture surface after aging between 500 and

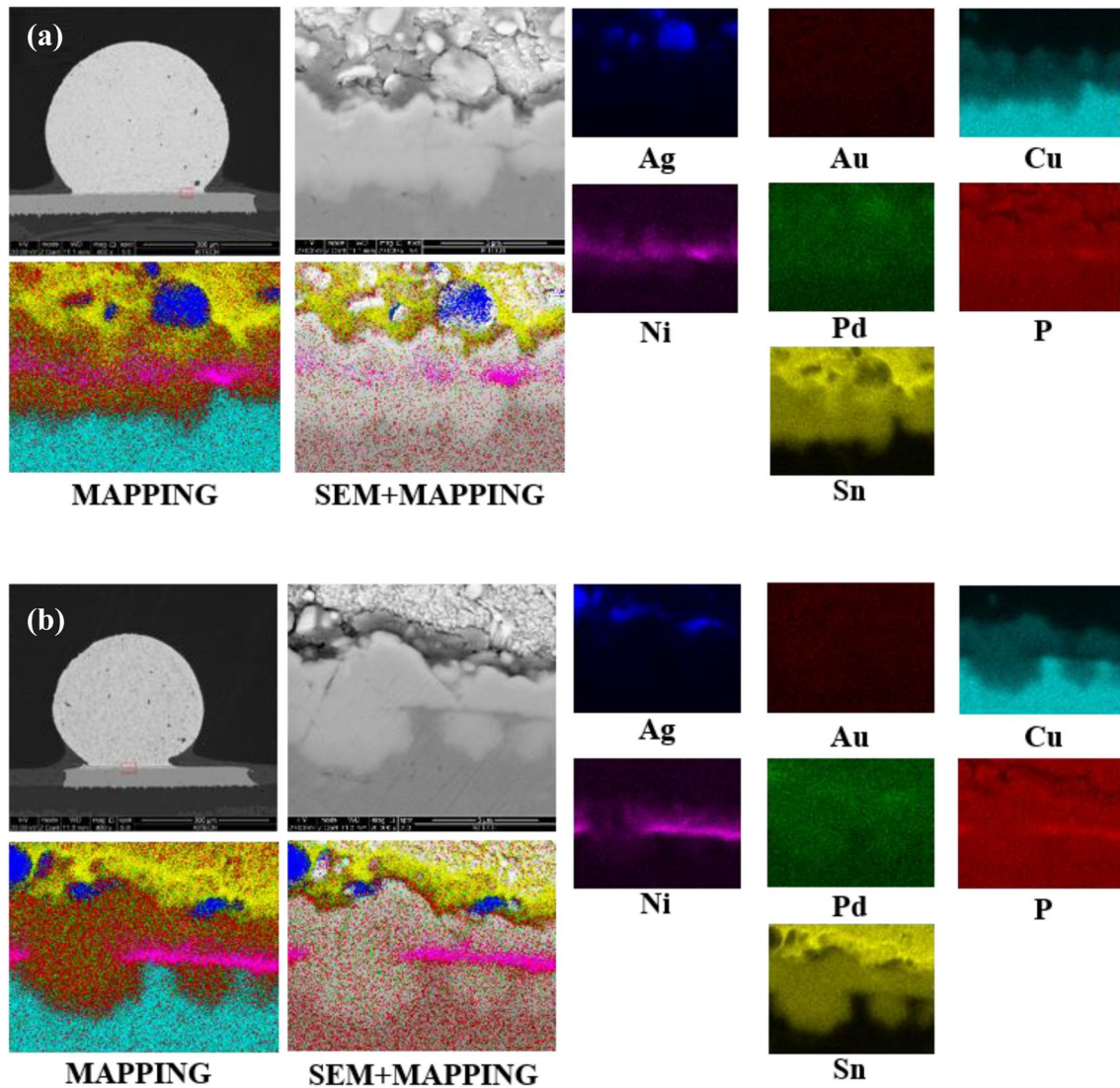


Fig. 8 SEM elemental mapping of Sn-3.0Ag-0.5Cu solder with Pd(P) containing thin ENEPIG surface-finished PCB joints after aging at 150 °C. **a** 100 h and **b** 250 h

1000 h. For the Pd(P) joints, the solder and $(\text{Cu,Ni})_6\text{Sn}_5$ IMC surface were observed on the fracture surface after reflowing (Fig. 11f). After aging for 100 h, the $(\text{Cu,Ni})_6\text{Sn}_5$ IMC surface occupied approximately a quarter of the fracture surface (Fig. 11g). After aging for 250 h, the area of the $(\text{Cu,Ni})_6\text{Sn}_5$ IMC surface slightly increased on the fractured surface (Fig. 11h). However, the area of the fractured $(\text{Cu,Ni})_6\text{Sn}_5$ IMC did not significantly increase after aging between 250 and 1000 h. These fracture analysis results are consistent with the high-speed shear strength results (Fig. 10a).

Figure 12 shows the top view SEM micrographs of the pure Pd and Pd(P) joints after low-speed shear testing. Most of the fracture surface for both the pure Pd and Pd(P) joints after low-speed shear testing were comprised of a Sn-rich matrix with a ductile fracture mode. The initial decrease in

the low-speed shear strength (Fig. 10b) was mainly due to the softening of the solder matrix during isothermal aging at 150 °C [22, 44].

Figure 13 shows the brittle fracture rate of the pure Pd and Pd(P) joints as a function of aging time after high-speed shear testing. The brittle fracture rate of the pure Pd joint was less than 10% after aging for 100 h but increased with increasing aging time, up to about 60%. In contrast, the Pd(P) joint had a higher brittle fracture rate during the initial aging stage. However, the magnitude of the brittle fracture rate increase was not significant with increasing aging time. The brittle fracture rate of the Pd(P) joint after aging for 1000 h was about 40%.

Force–displacement ($F-x$) curves for the pure Pd and Pd(P) joints after high-speed and low-speed shear testing

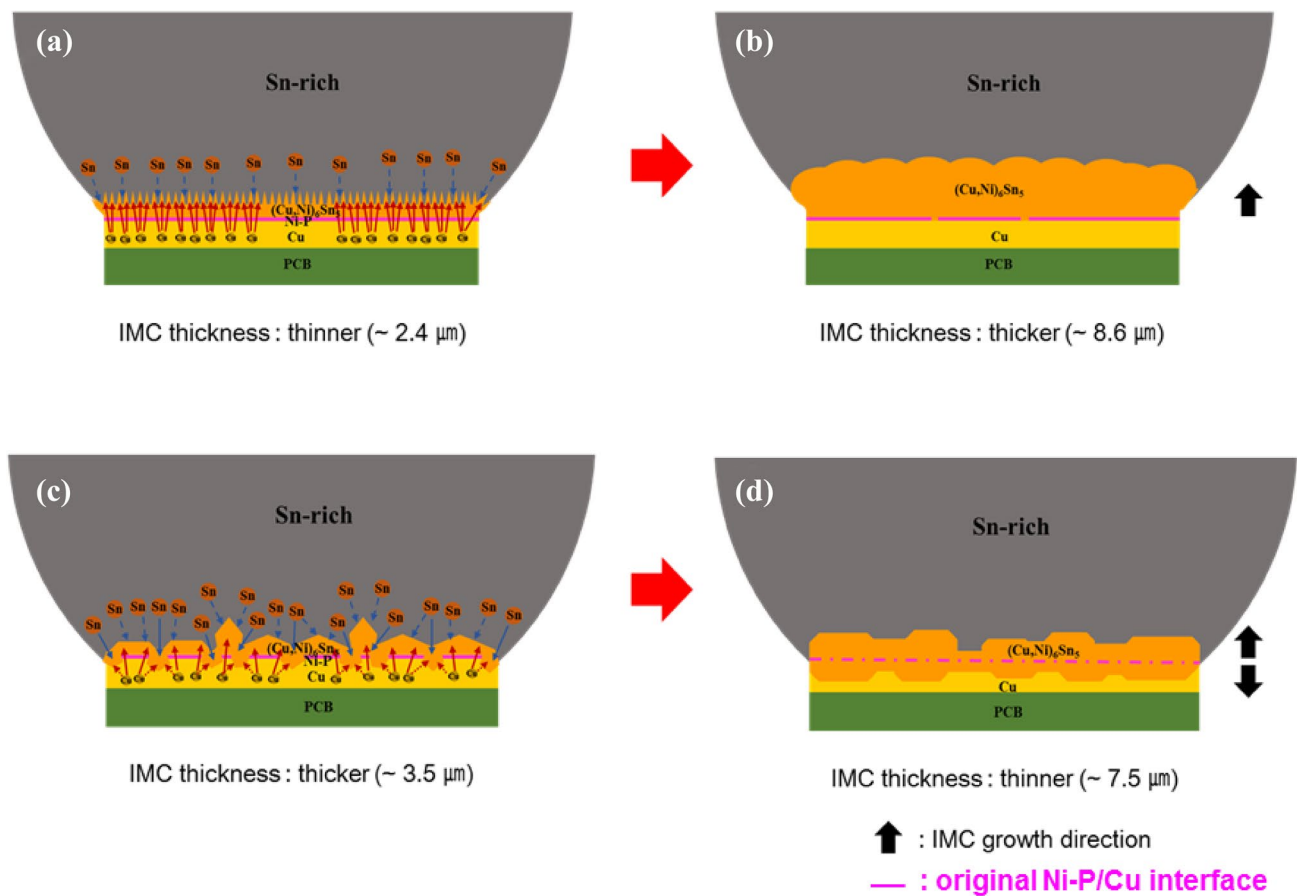


Fig. 9 Schematic diagrams of sequential interfacial reactions of the Sn–3.0Ag–0.5Cu solder. **a** and **b** Pure Pd joint, **c** and **d** Pd(P) joint, **a** and **c** 100 h aging, and **b** and **d** 500 h aging

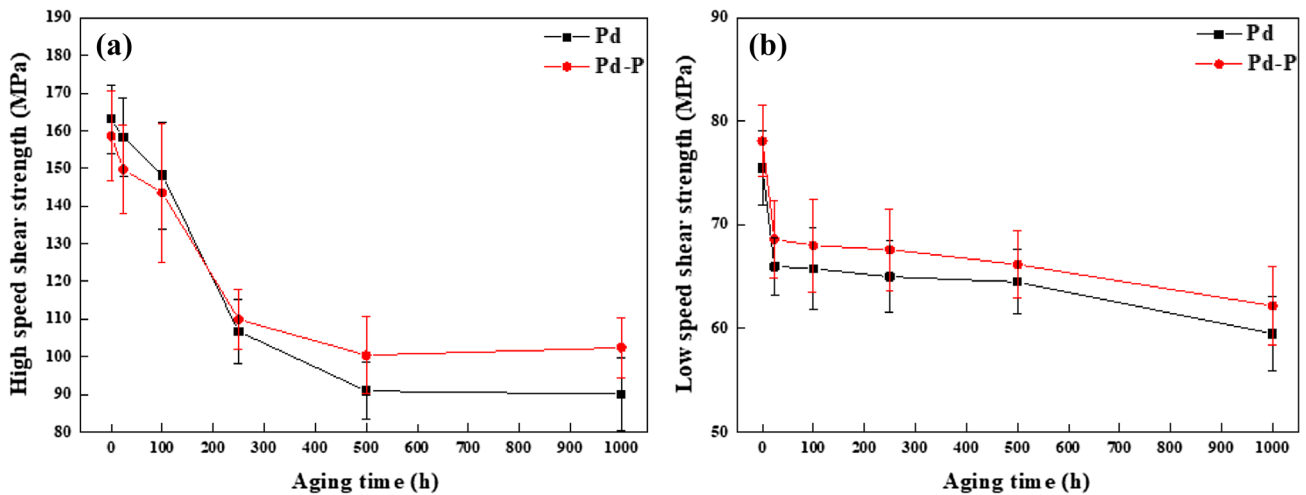


Fig. 10 Shear strength of Sn–3.0Ag–0.5Cu solder with pure Pd and Pd(P) containing thin ENEPIG surface-finished PCB joints as a function of aging time. After **a** high-speed and **b** low-speed shear testing

are shown in Fig. 14. As shown in Fig. 14a and b, both the pure Pd and Pd(P) joints were similar to the reflowed joints after aging for 100 h. After the high-speed shear test,

the high-speed shear strength and distance of both the pure Pd and Pd(P) joints (Fig. 14a, b) were gradually decreased from approximately 160 MPa to about 90 or 110 MPa,

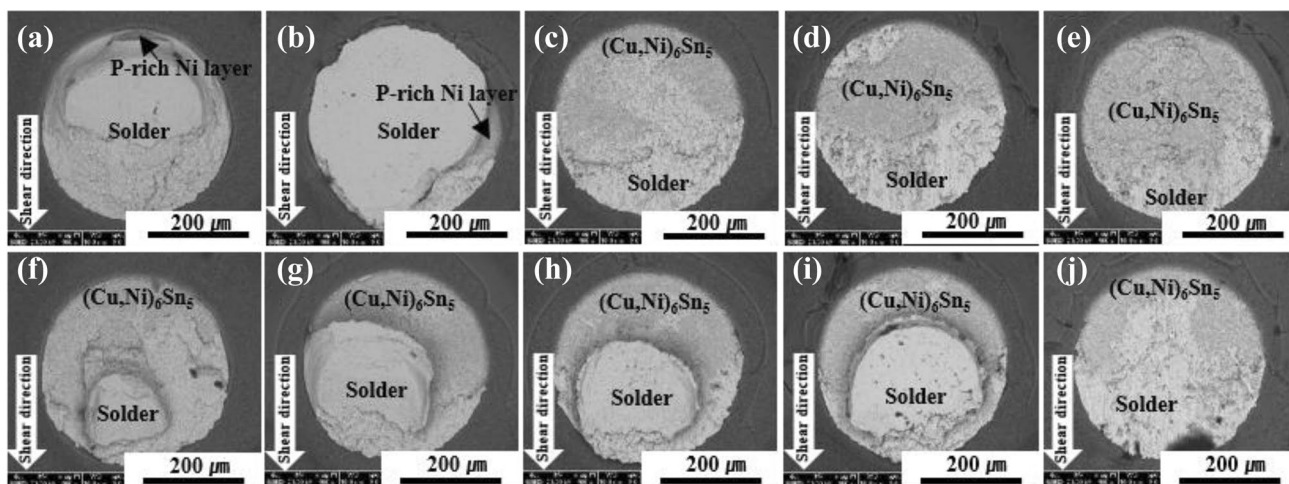


Fig. 11 Top view SEM micrographs of Sn-3.0Ag-0.5Cu solder with pure Pd or Pd(P) containing thin ENEPIG surface-finished PCB joints after high-speed shear testing. **a–e** Pure Pd, **f–j** Pd(P), **a** and **f** after reflow, **b** and **g** 100 h, **c** and **h** 250 h, **d** and **i** 500 h, and **e** and **j** 1000 h

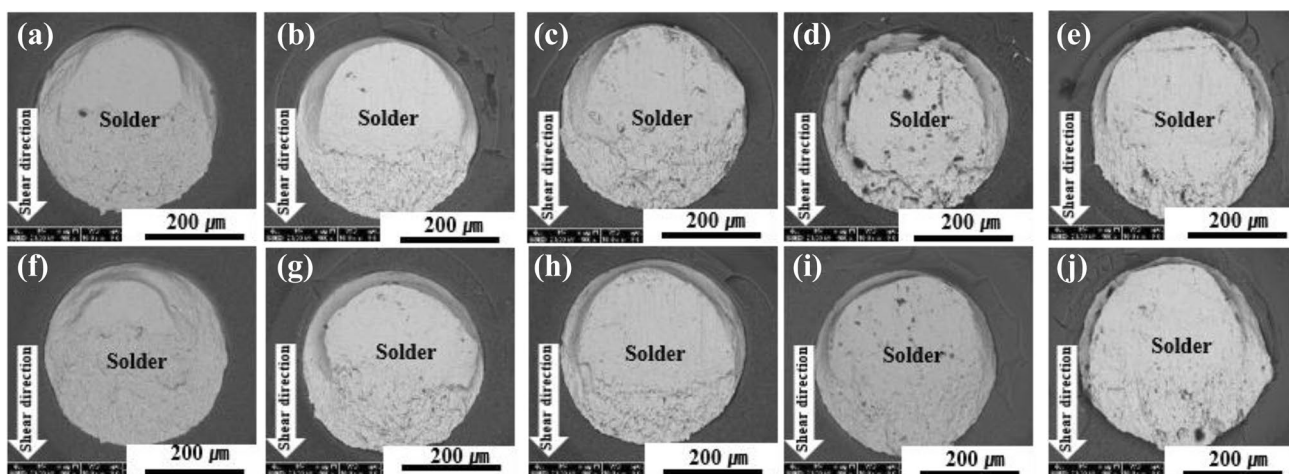


Fig. 12 Top view SEM micrographs of Sn-3.0Ag-0.5Cu solder with pure Pd or Pd(P) containing thin ENEPIG surface-finished PCB joints after low-speed shear testing. **a–e** Pure Pd, **f–j** Pd(P), **a** and **f** after reflow, **b** and **g** 100 h, **c** and **h** 250 h, **d** and **i** 500 h, and **e** and **j** 1000 h

with increasing aging time. The fracture energy ($F-x$ curve dimension) of the pure Pd joints was lower than that of the Pd(P) joint after each aging interval. Moreover, the shear strength of the pure Pd joints was evident as the stress rapidly dropped after the peak maximum with increasing aging time. However, the shear strength of the Pd(P) joints gradually decreased after peak maximum, regardless of aging time.

After the low-speed shear test, the $F-x$ curves of both the pure Pd and Pd(P) joints featured quite different shapes compared with those after the high-speed shear test. The shear strength reduction rate of both the pure Pd and Pd(P) joints after the low-speed shear test was lower than that of the high-speed shear test, regardless of aging time. In addition, the distance of the pure Pd and Pd(P) joints after the

high-speed shear test was rapidly shortened with increasing aging time, but that of the low-speed shear test showed similar results to those obtained after reflowing and aging for 1000 h. The reason for the difference in the $F-x$ curve shape according to the shear speed is that the thickness of the IMC is more susceptible to higher speed and the brittle fracture mode [43]. These $F-x$ analysis results are consistent with the results of interfacial IMC thickness (Fig. 6) and shear strength (Fig. 10). These different shaped $F-x$ curves and shear strength results relate to the deformation fracture modes. The fracture modes of both the pure Pd and Pd(P) joints after high-speed shear tests tend to increase the $(\text{Cu,Ni})_6\text{Sn}_5$ IMC fracture surface dimension, and a brittle fracture mode was observed. As mentioned before, the IMC thickness and shear strength are closely related, and the

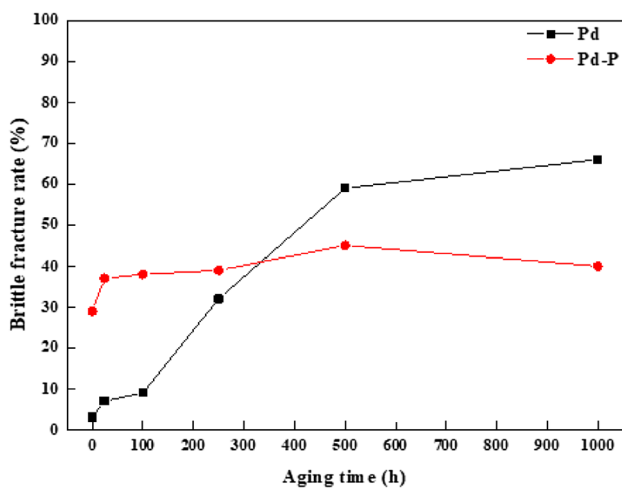


Fig. 13 Brittle fracture rate of Sn-3.0Ag-0.5Cu solder joints as a function of aging time after high-speed shear testing

shear strength values affect the fracture modes. The brittle fracture dimension of the pure Pd joint after aging for 250 h is larger than that of the Pd(P) joint, with similar results in high-speed shear strength. The fracture modes of the pure Pd and Pd(P) joints after low-speed shear tests were mostly solder surfaces with a ductile fracture mode.

On the other hand, typical ductile fracture curves were observed in the low-speed shear tests, as shown in Fig. 14c, d. As discussed, brittle fractures were not observed in the low-speed shear tests.

4 Conclusion

In this study, we compared the interfacial reactions and mechanical properties of a thin ENEPIG PCB substrate containing a pure Pd or Pd(P) layer with SAC305 solder joints after reflowing and aging treatment. A needle-type $(\text{Cu,Ni})_6\text{Sn}_5$ IMC and a P-rich Ni layer formed at the pure

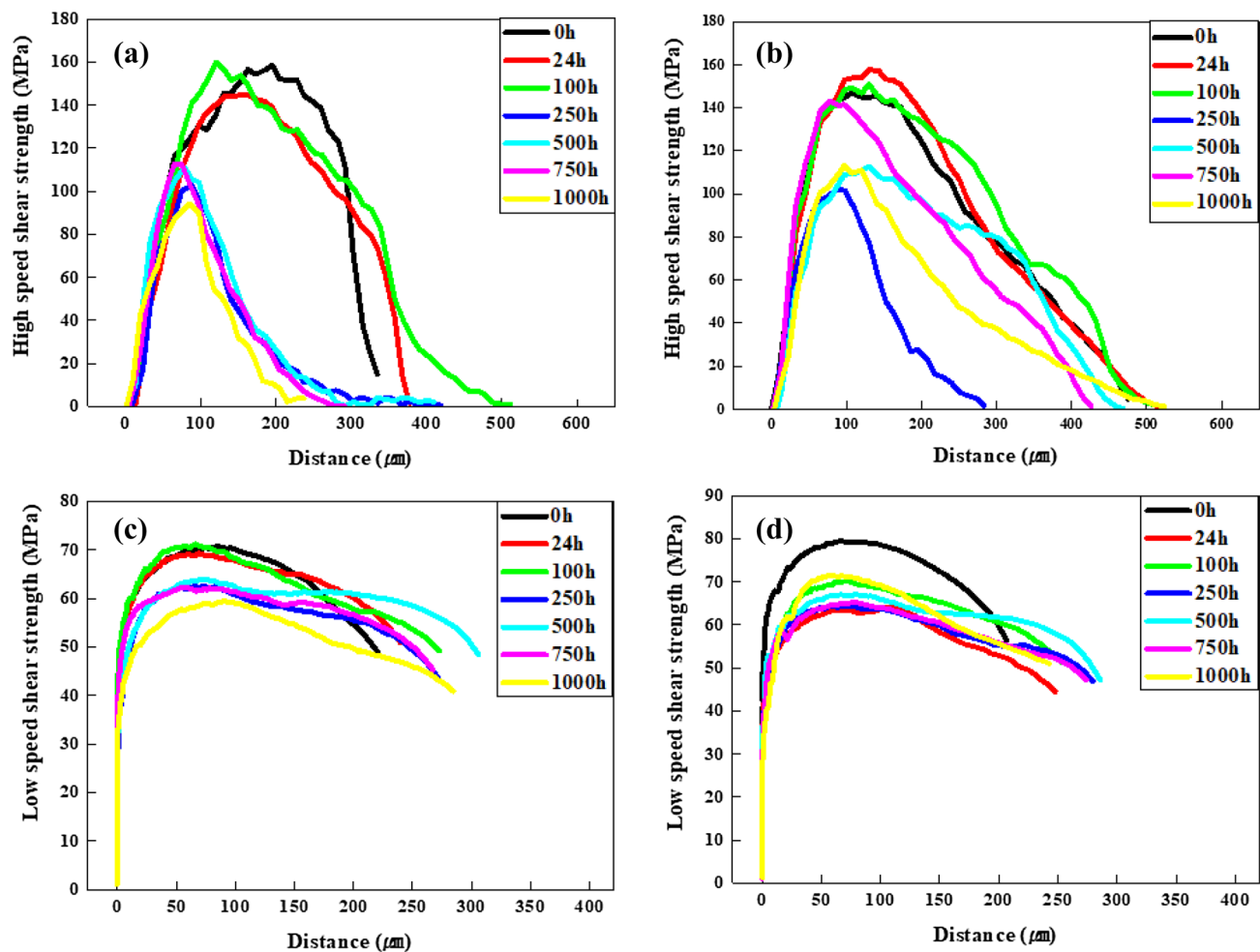


Fig. 14 F - x curves of Sn-3.0Ag-0.5Cu solder with pure Pd or Pd(P) containing thin ENEPIG surface-finished PCB joints after shear testing. **a** and **c** Pure Pd, **b** and **d** Pd(P), **a** and **b** high-speed shear testing, and **c** and **d** low-speed shear testing

Pd joint and a chunky-type $(\text{Cu,Ni})_6\text{Sn}_5$ IMC formed at the Pd(P) joint after reflowing. For both the pure Pd and Pd(P) joints, dominant $(\text{Cu,Ni})_6\text{Sn}_5$ IMCs grew as the aging time increased. The $(\text{Cu,Ni})_6\text{Sn}_5$ IMC of the pure Pd joint was slightly thinner than that of the Pd(P) joint after aging for 100 h. However, the $(\text{Cu,Ni})_6\text{Sn}_5$ IMC of the pure Pd joint was thicker than that of the Pd(P) joint after aging for 250 h. The growth rate of the interfacial IMC layer was mainly controlled by the IMC morphology and the main diffusion element during the aging treatment. In the pure Pd joints, the Cu in the substrate was continuously supplied to the interface and then the $(\text{Cu,Ni})_6\text{Sn}_5$ IMC grew in the direction of the solder. A relatively thick $(\text{Cu,Ni})_6\text{Sn}_5$ IMC layer formed in the pure Pd joint during aging. On the other hand, in the case of the Pd(P) joint, the rough and uneven-shaped top and bottom layers of $(\text{Cu,Ni})_6\text{Sn}_5$ IMC gradually increased with aging time.

High-speed shear test results revealed that the shear strength of the Pd(P) joint was lower than that of the pure Pd joint until an aging time of 100 h. However, the shear strengths of the Pd(P) and pure Pd joints overlapped between 100 and 250 h of aging. The low-speed shear strength of the Pd(P) joint was higher than that of the pure Pd joint for the whole aging time. In addition, the brittle fracture rate of the Pd(P) joint remained low (~40%) after a long aging duration (1000 h). Therefore, P in the Pd layer of the thin ENEPIG surface finish improved the interfacial microstructures and mechanical properties of the SAC305 solder joints after a long aging treatment.

Acknowledgements This work was supported by a research project grant from the Ministry of Trade, Industry and Energy, Republic of Korea [Grant Number 20003904].

References

1. Y.C. Chan, D. Yang, *Pro. Mater. Sci.* **55**, 428 (2010). <https://doi.org/10.1016/j.pmatsci.2010.01.001>
2. W.H. Chen, C.F. Yu, H.C. Cheng, Y.M. Tsai, S.T. Lu, *Microelectron. Eng.* **53**, 30 (2013). <https://doi.org/10.1016/j.microrel.2012.06.146>
3. T.K. Lee, H. Ma, K.C. Liu, J. Xue, *J. Electron. Mater.* **39**, 2564 (2010). <https://doi.org/10.1007/s11664-010-1352-8>
4. C.T. Peng, C.M. Liu, J.C. Lin, H.C. Cheng, *I.E.E.E. Trans. Electron. Packag. Manuf.* **27**, 684 (2004). <https://doi.org/10.1109/TCAPT.2004.838867>
5. J. Zhang, Z. Hai, S. Thirugnanansambandam, J.L. Evans, M.J. Bozack, Y. Zhang, J.C. Suhling, *I.E.E.E. Trans. Electron. Packag. Manuf.* **3**, 1348 (2013). <https://doi.org/10.1109/TCPMT.2013.2251932>
6. A.K. Gain, L. Zhang, *J. Alloys. Compd.* **617**, 779 (2014). <https://doi.org/10.1016/j.jallcom.2014.08.076>
7. W.R. Myung, Y. Kim, S.B. Jung, *J. Alloys. Compd.* **615**, s411 (2014). <https://doi.org/10.1016/j.jallcom.2014.01.078>
8. J. Glazer, *J. Electron. Mater.* **23**, 693 (1994). <https://doi.org/10.1007/BF02651361>
9. K. Chu, Y. Sohn, C. Moon, *Scr. Mater.* **109**, 113 (2015). <https://doi.org/10.1016/j.scriptamat.2015.07.032>
10. L. Yang, W. Zhou, Y. Ma, X. Li, Y. Liang, W. Cui, P. Wu, *Mater. Sci. Eng. A* **667**, 368 (2016). <https://doi.org/10.1016/j.msea.2016.05.015>
11. H.F. Zou, Q.K. Zhang, Z.F. Zhang, *Mater. Sci. Eng. A* **532**, 167 (2012). <https://doi.org/10.1016/j.msea.2011.10.078>
12. S. Ahat, M. Sheng, L. Luo, *J. Electron. Mater.* **30**, 1317 (2001). <https://doi.org/10.1007/s11664-001-0118-8>
13. X. Deng, G. Piotrowski, J.J. Williams, N. Chawla, *J. Electron. Mater.* **32**, 1403 (2003). <https://doi.org/10.1007/s11664-003-0108-0>
14. K. Zeng, K.N. Tu, *Mater. Sci. Eng. R* **38**, 55 (2002). [https://doi.org/10.1016/S0927-796X\(02\)00007-4](https://doi.org/10.1016/S0927-796X(02)00007-4)
15. Y.D. Jeon, A. Ostmann, H. Reichl, and K.W. Paik, in *2003 Electronic Components and Technology Conference Proceedings* (2003), pp. 1203–1208.
16. J.W. Yoon, Y.H. Lee, D.G. Kim, H.B. Kang, S.J. Suh, C.W. Yang, C.B. Lee, J.M. Jung, C.S. Yoo, S.B. Jung, *J. Alloys. Compd.* **381**, 151 (2004). <https://doi.org/10.1016/j.jallcom.2004.03.076>
17. H.W. Miao, J.G. Duh, *Mater. Chem. Phys.* **71**, 255 (2001). [https://doi.org/10.1016/S0254-0584\(01\)00298-X](https://doi.org/10.1016/S0254-0584(01)00298-X)
18. P.J. Shang, Z.Q. Liu, D.X. Li, J.K. Shang, *J. Electron. Mater.* **38**, 2579 (2009). <https://doi.org/10.1007/s11664-009-0894-0>
19. S.Y. Lee, H.M. Lee, J.H. Park, S.M. Shin, W.J. Kim, T. J. Choi, and K.W. Paik, in *2008 Electronic Components and Technology Conference Proceedings* (2008), pp. 649–654. <https://doi.org/10.1109/ECTC.2018.00103>
20. Y. Zhang, Z. Cai, J. C. Suhling, P. Lall, and M. J. Bozack, in *2008 Electronic Components and Technology Conference Proceedings* (2008), pp. 99–112. <https://doi.org/10.1109/ECT.2008.4549956>
21. A.A. El-Daly, Y. Swilem, M.H. Makled, M.G. El-shaarawy, A.M. Abdraboh, *J. Alloys. Compd.* **484**, 134 (2009). <https://doi.org/10.1016/j.jallcom.2009.04.108>
22. J.W. Yoon, B.I. Noh, Y.H. Lee, H.S. Lee, S.B. Jung, *Microelectron. Reliab.* **48**, 1864 (2008). <https://doi.org/10.1016/j.microrel.2008.07.065>
23. D. Herkommer, J. Punch, M. Reid, *Microelectron. Reliab.* **50**, 116 (2010). <https://doi.org/10.1016/j.microrel.2009.08.008>
24. D.A. Shnawah, M.F.M. Sabri, A. Badruddin, *Microelectron. Reliab.* **52**, 90 (2012). <https://doi.org/10.1016/j.microrel.2011.07.093>
25. A.K. Gain, T. Fouzder, Y.C. Chan, W.K.C. Yung, *J. Alloys. Compd.* **509**, 3319 (2011). <https://doi.org/10.1016/j.jallcom.2010.12.048>
26. G. Ju, X. Wei, J. Liu, *Solder. Surf. Mt. Technol.* **20**, 4 (2008). <https://doi.org/10.1108/09540910810885660>
27. A.K. Gain, Y.C. Chan, *Intermetallics* **29**, 48 (2012). <https://doi.org/10.1016/j.intermet.2012.04.019>
28. P. Liu, P. Yao, J. Liu, *J. Alloys. Compd.* **470**, 188 (2009). <https://doi.org/10.1016/j.jallcom.2008.02.102>
29. R. Zhang, F. Guo, J. Liu, H. Shen, F. Tai, *J. Electron. Mater.* **38**, 241 (2009). <https://doi.org/10.1007/s11664-008-0582-5>
30. S.J. Wang, C.Y. Liu, *Scr. Mater.* **49**, 813 (2003). [https://doi.org/10.1016/S1359-6462\(03\)00486-X](https://doi.org/10.1016/S1359-6462(03)00486-X)
31. M.S. Kim, H. Nishikawa, *Microelectron. Reliab.* **76–77**, 420 (2017). <https://doi.org/10.1016/j.microrel.2017.06.083>
32. K. Zeng, R. Stierman, D. Abbot, and M. Murtuza, in *10th Inter-society Conference on Phenomena in Electronic Systems conference Proceedings*, (2006) pp. 1111–1119. <https://doi.org/10.1109/ITHERM.2006.1645469>
33. C.F. Tseng, T.K. Lee, G. Ramakrishna, K.C. Liu, J.G. Duh, *Mater. Lett.* **65**, 3216 (2011). <https://doi.org/10.1016/j.matlet.2011.07.015>

34. J.W. Yoon, B.I. Noh, J.H. Yoon, H.B. Kang, S.B. Jung, J. Alloys. Compd. **509**, L153 (2011). <https://doi.org/10.1016/j.jallcom.2011.01.015>
35. J.W. Yoon, B.I. Noh, S.B. Jung, J. Electron. Mater. **40**, 1950 (2011). <https://doi.org/10.1007/s11664-011-1686-x>
36. Chaillot, N. Venet, P.E. Tegehall, J. Hokka, and J.L. Lortal, in *2013 European Microelectronics Packaging Conference (EMPC) proceedings*, (2013) pp. 1–6.
37. K.P.L. Pun, M.N. Islam, J. Rotanson, C.W. Cheung, A.H.S. Chan, J. Electron. Mater. **47**, 5191 (2018). <https://doi.org/10.1007/s11664-018-6385-4>
38. J. Palmer, D. Chu, and L. Fang, in *Electronic Components and Technology Conference (ECTC) proceedings*, (2012), pp. 1159–1162. <https://doi.org/10.1109/ECTC.2012.6248982>.
39. L.B. Belykh, N.I. Skripov, T.P. Sterenchuk, V.V. Akimov, V.L. Tauson, F.K. Schmidt, Russ. J. Gen. Chem. **86**, 1454 (2016). <https://doi.org/10.1134/S1070363216090073>
40. C.E. Ho, L.H. Hsu, C.H. Yang, T.C. Yeh, P.T. Lee, Thin Solid Films **584**, 257 (2015). <https://doi.org/10.1016/j.tsf.2014.12.026>
41. C.Y. Ho, J.G. Duh, C.W. Lin, C.J. Lin, Y.H. Wu, H.C. Hong, T.H. Wang, J. Mater. Sci. **48**, 2724 (2013). <https://doi.org/10.1007/s10853-012-7070-2>
42. C.E. Ho, C.W. Fan, W.Z. Hsieh, Surf. Coat. Tech. **259**, 244 (2014). <https://doi.org/10.1016/j.surfcoat.2014.04.027>
43. S.S. Ha, J.K. Jang, S.O. Ha, J.W. Kim, J.W. Yoon, B.W. Kim, S.K. Park, S.B. Jung, J. Electron. Mater. **38**, 2489 (2009). <https://doi.org/10.1007/s11664-009-0916-y>
44. J.W. Yoon, B.I. Noh, S.B. Jung, I.E.E.E. Trans. Comp. Packag. Technol. **33**, 222 (2010). <https://doi.org/10.1109/TCAPT.2009.2028134>

Publisher's Note Springer Nature remains neutral with regard to jurisdictional claims in published maps and institutional affiliations.